Formation Mechanism of Band Delta-Ferrite in 416 Stainless Steel and Its Relationship with MnS and $M_{23}C_6$

Yi Wang, Qianren Tian, Xiangyu Xu, and Jianxun Fu

Abstract AISI 416 steel with a banded structure (BS) that is formed by element segregation, and its MnS significantly affects its microstructure and properties during the hot working process. In this study, we investigated the formation mechanism of the BS and its relationship with MnS in 416 steel by carrying out thermodynamic calculations and microscopic characterization measurements. The BS was identified to be a delta-ferrite phase rich in Cr. In addition, when the volume fraction of delta-ferrite was the largest during the 1665 K, the BS was most likely to precipitate. The fine $M_{23}C_6$ particles around the BS enhanced the segregation of Cr and worked with the MnS inclusions to pin the surrounding grains. The metastable-banded structure formed near the BS transformed into a martensite phase. The MnS inclusions pinned and refined the grains and showed four types of distributions.

Keywords 416 stainless steel · Banded structure · Segregation · MnS inclusion · $M_{23}C_6$ · Pinning effect

Introduction

AISI 416 is a typical sulfur-containing, free-cutting stainless steel with an effective cutting performance. It is often used to make free-cutting parts, such as solenoid valves, micromotors, and electrical components [1]. The cutting performance of 416 free-cutting steel mainly depends on the distribution of its secondary phase particles, that is, the distribution uniformity and cutting morphology of MnS inclusions. When MnS inclusions stretch in the rolling direction during the rolling process, they can easily cause cracks in the rolled material and deteriorate its transverse properties [2].

Y. Wang · Q. Tian · X. Xu · J. Fu (✉)
Center for Advanced Solidification Technology (CAST), School of Materials Science and Engineering, Shanghai University, Shanghai 200444, China
e-mail: fujianxun@shu.edu.cn

State Key Laboratory of Advanced Special Steel, Shanghai University, Shanghai 200444, China

It is believed that the formation of the BS in steel is closely related to the evolution of the segregated elements. Hence, the impact of these elements should not be ignored. Therefore, in this study, we carried out phase transition analyses and thermodynamics calculations to investigate the evolution of the microstructure and secondary phase particles in steel at the rolling temperature. A high-temperature confocal laser scanning microscopy (CLSM) analysis was performed during the heating–preservation–cooling process at the hot working temperature (1170 °C, 1443 K). Electron backscatter diffraction (EBSD), scanning electron microscopy (SEM), and electron probe microanalyzer (EPMA) measurements were performed to analyze the formation mechanism of the BS in the steel and its relationship with the segregation elements, Cr and C, and secondary phase particles, MnS and $M_{23}C_6$.

Experimental

Chemical Composition

AISI 416 stainless steel samples were taken from rolled products, and their metal and phosphorus contents were determined using a direct-reading spectrometer (Model: Spectro, SPECTROMAXx). The carbon and sulfur contents of the steel were determined using a carbon sulfur analyzer (Model: NCS, CS-2800).

Room Temperature Observation

In this experiment, a metallographic microscope (Model: Zeiss, Axio Observer) was used to observe the metallographic surface of the sample to ensure that it had no obvious scratches that may affect the high-temperature experiment observations.

The morphologies and compositions (in atomic percent, at %) of the inclusions and steel were nalyse using a scanning electron microscope (Model: Phenom, Pro X) equipped with an energy-dispersive spectrometer. An EPMA (Model: Shimadzu, 8050G) was used to o nalyse the distribution of the segregated elements accurately and examine the changes in the elemental compositions of the ferrite and martensite phases by element mapping. EBSD was used to examine the microstructures of the specimens before and after the CLSM experiments at an accelerating voltage of 20 keV and a step of 0.25 μm on each sputtering plane. A rectangular scanning grid (60 μm × 45 μm) was used to perform the EBSD measurements.

Fig. 1 Heat treatment curves of in situ observations for the experimental (red) and controlling (black) temperatures
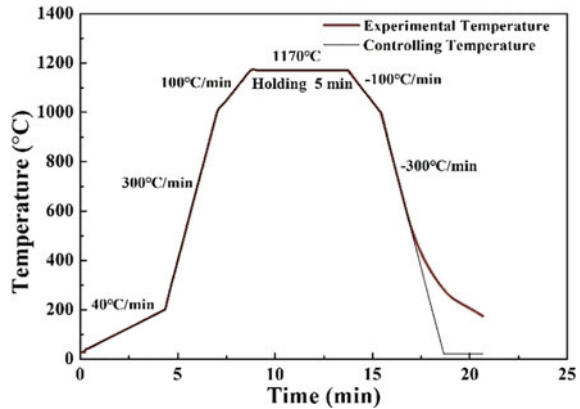
High-Temperature Observation

After the metallographic microscope observation, the specimen was placed in a corundum crucible with an inner diameter of 8 mm, an outer diameter of 9 mm, and a height of 3.5 mm. The crucible was then placed in a CLSM thermal treatment furnace (Lasertec, Model: VL2000DX-SVF17SP). The thermal treatment furnace was evacuated using a vacuum pump, and argon gas was injected into the furnace. During the thermal treatment of the specimen, the evolution behaviors of the steel matrix and MnS inclusions were observed. The temperature control curve of the specimen is shown in Fig. 1.

Results and Discussion

Phase Composition

The chemical composition of the steel is presented in Table 1. The steel consisted of 0.1%, 1.25%, 0.33%, 13%, and 0.5% of C, Mn, S, Cr, and Ni, respectively. The high Mn and S contents of the steel provided favorable conditions for the precipitation and formation of MnS inclusions, which acted as a free-cutting phase in the steel.

Prior to the CLSM analysis, EBSD measurements were carried out to examine the structure of the specimen, and the results are shown in Fig. 2. The area indicated by the white arrow in Fig. 2a represents the BS, and the surrounding acicular

Table 1 Chemical composition of 416 stainless steel (in mass%)

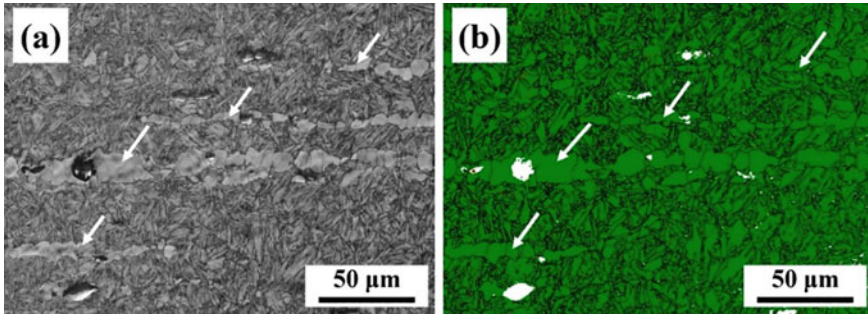| Composition	C	Si	Mn	P	S	Cr	Ni	Mo
Content	0.10	0.75	1.25	0.06	0.33	13.00	0.50	≤ 0.30

Fig. 2 EBSD analysis of the banded microstructure prior to the CLSM analysis: **a** Kikuchi belt contrast diagram**; b** phase distribution. The write arrows indicate the BSs

structure represents the martensite phase. As can be observed from the phase distribution diagram shown in Fig. 2b, the BS and martensite phase are indicated by the same color. This indicates that both the BS and martensite phase showed the body-centered cubic (BCC) structure. Moreover, the white secondary phase was composed of spherical or ellipsoidal MnS inclusions and $M_{23}C_6$, as confirmed in Sect. 3.2.2.

Based on the chemical composition results, the equilibrium phase transition of the 416 stainless steel over the temperature range of 927–1527 °C (1200–1800 K) was examined using Thermo-Calc software, and the results are shown in Fig. 3. Figure 3(a) shows that during the cooling process, the molten steel content began decreasing at 1481 °C (1754 K), and the volume fraction of the high-temperature δ-Fe phase increased gradually. The volume ratio of the two phases was almost the same at 1457 °C (1730 K). At this temperature, the MnS inclusions began precipitating and grew until their content increased to 1.12%. At 1392 °C (1665 K), the content of δ-Fe was the largest; the content of liquid steel was the smallest, and the face-centered cubic austenite ferrite (FCCγ-F**e**) phase began precipitating. The temperature difference required for the δ-Fe**-**to**-γ-**Fe transformation was larger than that required for the liquid steel-to**-**δ-Fe transformation. Therefore, δ-Fe almost completely transformed into γ-Fe at 1124 °C (1397 K).

The changes in the Cr and C contents of the liquid, BCC, and FCC phases were also analyzed, as shown in Fig. 3b. With a decrease in temperature, the Cr and C contents of the solid–liquid two-phase region (L + δ, gray-shaded part) increased; however, the increase was faster in the liquid phase than that in the δ-Fe phase. In the δ-Fe + γ-Fe two-phase region (yellow shaded part), the Cr content increased, while the C content decreased when moving from the δ-Fe to γ-Fe phase. The Cr content of the BCC phase was higher than that of the FCC phase. At the same temperature, the C content of the FCC phase was higher than that of the BCC phase. During the transformation of Cr from δ-Fe to γ-Fe, severe segregation of Cr occurred in the BCC phase, and the segregation of C occurred in the FCC phase. As can be observed from the phase composition results shown in Fig. 3a, the BS was most likely to be formed when the δ-Fe volume percentage was the largest, that is, at approximately 1392 °C. This implies that for most martensitic stainless steels, such as 410 and 420 stainless
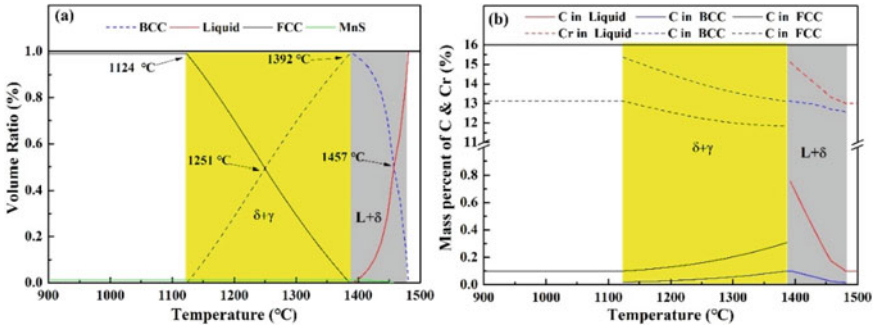
Fig. 3 Phase diagram and elemental analysis of the AISI 416 stainless steel **a** phase composition as a function of temperature; **b** elemental composition of the phases as a function of temperature

steels, the formation of this banded ferrite (BF) structure is unavoidable during the transformation of δ-Fe to γ-Fe and then to martensite.

Evolution and Characteristics of the BS

Heating–Preservation–Cooling Process

In the high-temperature confocal experiment, the holding temperature was set at the hot working temperature (1170 °C), and the microstructure evolution process of the sample during the heating, preservation, and cooling processes is shown in Fig. 4. In the SEM images (Sect. 3.3), the gray area represents the steel matrix and the black spherical or ellipsoidal secondary phase particles represent MnS inclusions.

As shown in Fig. 4a, the system started heating up at room temperature (26.7 °C, 299.7 K). According to statistics, a total of 29 inclusions were counted in the field of view. These inclusions had an average equivalent diameter of 3.73 µm, a length of 7.16 µm, a width of 2.3 µm, an aspect ratio of 3.11, and a density of 76.3/mm^2. The largest ellipsoidal MnS inclusions had a length of approximately 20 µm and width of 6 µm, while the smallest inclusions were nanoscale precipitates.

These nanoscale precipitates played an important role in the subsequent evolution of the assembly. As the temperature increased gradually to above the austenitizing temperature, the BSs parallel to the long side of the inclusions appeared. The BSs were denoted as BF1–BF4 from top to bottom, as shown in Fig. 4b. In addition, many small secondary phase particles appeared on the left side of BF2, as indicated by the green arrow. When the temperature increased to 1170 °C, a clearer BS appeared. From the CLSM two-dimensional perspective, the gradual increase in the area of the BS indicates that the BF grains grew after reaching the temperature of the two-phase region from a three-dimensional perspective, as shown in Fig. 4c. Among all the BSs investigated, BF1 was the thinnest with the smallest grains and the lowest number of
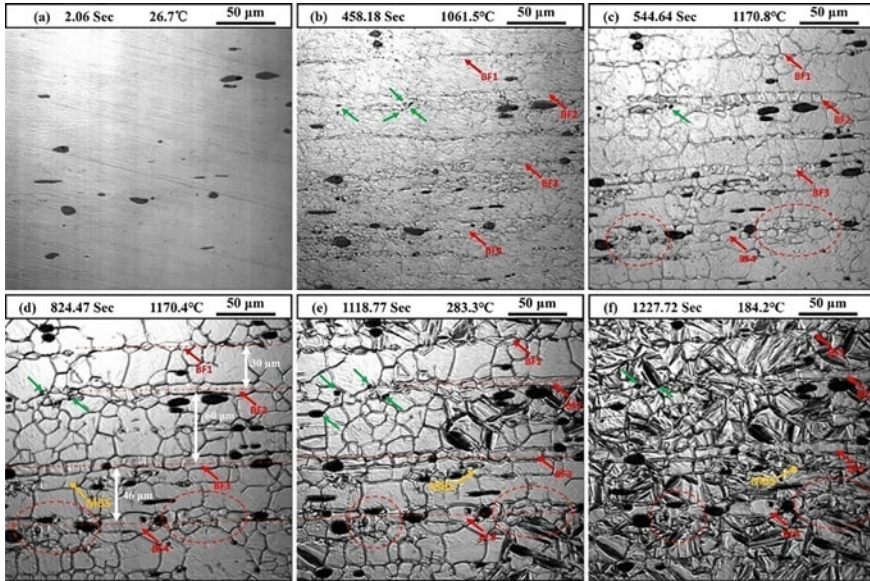
Fig. 4 Phase change of 416 stainless steel during the heating and cooling processes, as observed using CLSM **a** at room temperature; **b** during the heating process; **c** at the beginning of the heat preservation process; **d** during heat preservation; **e** at the beginning of the cooling process; **f** at the end of the cooling process. The red, green, yellow, and white arrows denote the BFs, fine MnS grains, MBS, and distances between the BFs, respectively

inclusions around it. BF2 showed clearer BS morphology; moreover, the presence of fine MnS inclusion particles led to the refinement of the surrounding grains, which prevented the diffusion of elements in the BS along its length, thus blocking its expansion and reducing its length. This indicates that the fine and diffused MnS inclusions not only facilitated grain refinement, but also reduced the length of the BS. These inclusions also showed the pinning effect. In BF4, the four inclusion particles refined the grains in the BS, and the grain size was significantly smaller than those of the other BSs, as shown by the dotted circle in Fig. 4c.

During the heat preservation process, as shown in Fig. 4d, each grain in the BS grew gradually and could be clearly observed. The length and width of each grain in the BS were approximately 15–20 and 5 μm, respectively. The red dashed lines represent the centerlines of the BFs, and the spacings between BF1 and BF2, BF2 and BF3, and BF3 and BF4 were 30, 60, and 42 μm, respectively. It should be noted that a metastable banded structure (MBS) with a width of approximately 10 μm was formed under BF3 (the side with fewer MnS inclusions), as shown by the yellow arrow in Fig. 4. The grains of the MBS were larger than those of BF3.

When the steel matrix underwent phase transformation at 283.3 °C (556.3 K), as shown in Fig. 4e, the coarser grains initially transformed into martensite, subsequently, as the temperature continued to decrease, the smaller grains also showed transformation. When temperature decreased rapidly to 184.2 °C (457.2 K), as shown

in Fig. 4f, the ridgeline of the martensite phase was preferentially formed around the fine and dispersed particles, indicating that the particles on the left side of BF2 induced the martensite transformation effect. After heat preservation and cooling, the BS became slightly thinner; however, it retained the BF morphology, indicating that it was difficult to deteriorate this structure by heat treatment. At the same time, the MBS completely underwent martensitic transformation, which can be attributed to the downward diffusion of the segregated elements in BF3. The inclusions beneath the metastable structure prevented the further diffusion of the diffusing elements downward. Therefore, it can be stated that the MBS was formed due to the segregation elements. The transformation of the MBS to the martensite phase was caused by the insufficient concentration of the segregated elements in the structure.

Element Segregation of BS

As shown in Fig. 2, EBSD was used to analyze the difference in the steel matrix structure of the BS and its surrounding martensite after the heat treatment process. The results are shown in Fig. 4. The BSs in steel are indicated by the white arrows in the contrast diagram of the Kikuchi belt in Fig. 5a. The remaining acicular structure was martensite. According to the phase distribution diagram shown in Fig. 5b, the BS and martensite phase showed the BCC structure, indicating that there was no residual austenite in the steel. Based on the EBSD results (Fig. 2), phase diagram, and microstructure evolution analysis results, it can be stated that the heat preservation treatment at 1170 °C could barely improve the shape of the banded δ-Fe.

The phase transformation and changes in the elemental composition, evident from the phase diagram shown in Fig. 3, indicate that the steel showed high Cr (13%) and Mn (1.25%) contents, which caused the segregation of Cr and Mn. Therefore, an EPMA was used to determine the compositions of the segregated elements in the BS.
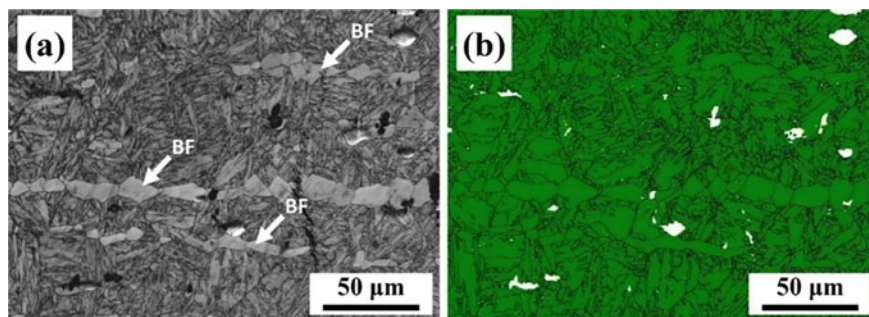

Fig. 5 EBSD analysis of the banded microstructure after the CLSM analysis: **a** Kikuchi belt contrast diagram; **b** phase distribution. The white arrows denote the BFs
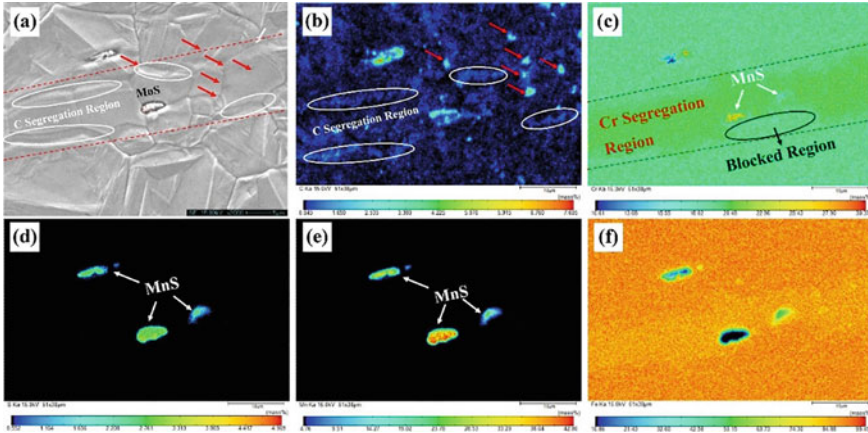
Fig. 6 EPMA elemental mapping of the banded microstructure **a** image; **b** C; **c** Cr; **d** Mn; **e** S; **f** Fe, the red and white arrows denote the carbides and MnS inclusions, respectively; the white and black circles denote the C segregation regions and the blocked region formed by the MnS inclusions, respectively

The EPMA scanning results of the specimen after CLSM are shown in Fig. 6. No segregation of Mn was observed in the BS, and the segregation was shown mainly by Cr and C. The segregation of C was mainly along the outer edge of the grain boundary of the BS and formed a carbon segregation zone with a width of approximately 2 μm, as indicated by the white arrows and circles in Figs. 6a and b. Although the segregation of C was not caused by the segregation of Mn, according to the scanning analysis of Mn and S, C showed a significant segregation near the MnS inclusions. The red arrows indicate the segregation points of C. $M_{23}C_6$ carbides may have formed outside the Cr segregation zone.

The diffusion rates of C and Cr under the heat preservation conditions are calculated using Eqs. (1) and (2), respectively [3, 4].

$$D_C^\gamma = 0.0761 \cdot EXP(-134429/RT) \tag{1}$$

$$D_{Cr}^\gamma = 0.0012 \cdot EXP(-219000/RT) \tag{2}$$

where D_C^γ and D_{Cr}^γ denote the diffusion coefficients (cm^2/s) of C and Cr in γ-Fe, respectively, R is the gas constant (8.314 J/(mol·K)), and T is the temperature (K).

At a certain austenitizing temperature, the diffusion rate of Cr was much lower than that of C. Therefore, when C segregated at the outer edge of the Cr segregation zone, it formed a segregation zone, as shown in Fig. 6b. This segregation of C resulted in the formation of many fine and dispersed carbides ($M_{23}C_6$) around the BS. These carbides showed the pinning effect around the Cr segregation zone [5, 6], limiting the elemental diffusion and preventing the formation of coarse grains.

In the Cr segregation zone, there were two types of MnS inclusions, larger and smaller, and Cr was concentrated around the larger MnS inclusions (approximately 5 µm in length and 3 µm in width), as shown in Fig. 6c. An obstructive zone with a length of approximately 15 µm and a width of approximately 5 µm was formed beneath the MnS inclusions, indicating that the MnS inclusions pinned the elemental diffusion. Wang et al. [7] reported that large MnS inclusions hinder the diffusion of alloying elements, thereby accumulating a banded degree, while small MnS inclusions have an insignificant effect on the large-scale diffusion of alloying elements. The EPMA results suggested that the smaller carbides and larger inclusions combined together to block the diffusion of elements. Mn did not segregate in the BS and only precipitated in the form of MnS inclusions on the grain boundaries of the BS and martensite phase, as shown in Fig. 6d–f.

Pinning Effect of the MnS Inclusions

Based on the location, MnS inclusions in 416 free-cutting stainless steel can be divided into four categories: those existing between two grain boundaries, between polycrystalline boundaries, within the grains, and throughout the grains. Different inclusions observed in this study, A–I, are shown in Fig. 7, and the elemental compositions of these inclusions are listed in Table 2. The EDS results showed that the inclusions far away from the Cr segregation zone, for example, inclusion I (approximately 20 µm away from the segregation zone) consisted of only a few Cr atoms. Inclusions A, C, D, F, G, and H present at the phase interface had more Cr atoms, while inclusions B and E observed within the grains had fewer Cr atoms. This indicates that the inclusions at the phase interface prevented the diffusion of segregated Cr to their other side, while the inclusions present within the grains could not prevent the diffusion of Cr. This is consistent with the EPMA results.

Affected by rolling, the long axis of the MnS inclusions in the grain boundaries is parallel to the long axis of the BS. Inclusion A, which exists between two grain boundaries, is a spherical MnS particle with a diameter of approximately 6 µm. Because of the pinning of this inclusion, the growth of the grains (with an equivalent diameter of approximately 10 µm) on both of its sides adds to the difficulty of forming larger grains. Therefore, the smaller grains caused significant squeezing of the MnS inclusions, making one of their ends sharp to impart a drop shape.

Conclusion

(1) The BS of the steel was identified to be a δ-Fe phase rich in Cr. When the δFe volume fraction was the largest during the solidification process (at 1392 °C (1665 K)), the length and width of each grain in the BS were approximately 15–20 and 5 µm, respectively, and the BS was most likely to precipitate.
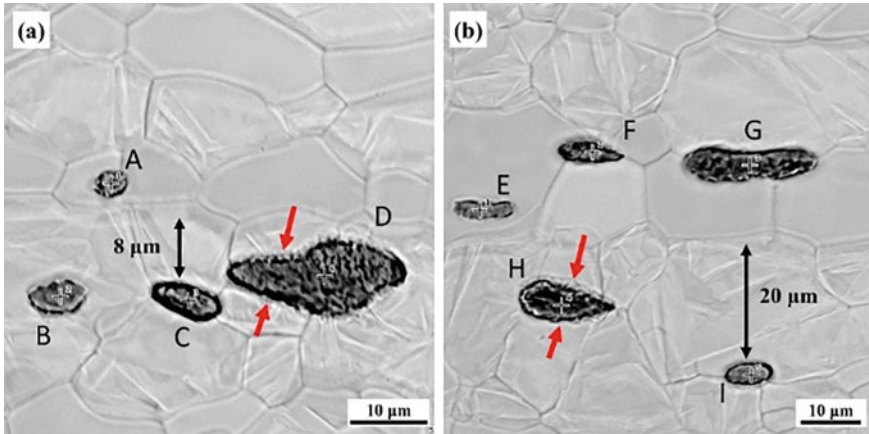
Fig. 7 MnS inclusions at the martensite-ferrite interface at room temperature **a** scene 1; **b** scene 2. The red and black arrows denote the extrusion direction of the grains to the inclusions and the distance between the MnS inclusions and BS, respectively

Table 2 Elemental composition of the inclusions

Inclusion	Elements (at%)			
	Mn	S	Cr	Fe
A	34.30	17.95	38.82	8.93
B	36.15	28.73	27.53	7.60
C	29.97	10.89	47.34	11.81
D	36.40	6.30	39.40	8.27
E	34.29	26.80	22.70	16.22
F	34.45	8.03	46.29	11.22
G	33.47	14.21	43.07	9.26
H	34.98	10.69	35.08	11.62
I	36.88	29.21	22.99	10.92

(2) The heat preservation treatment at 1170 °C (1443 K) could barely change the BS shape because the MnS inclusions and fine $M_{23}C_6$ carbides hindered the diffusion of Cr into the BS and pinned the BS grains, so that the surrounding grains did not coarsen during the heating process. The pining effect of the MnS inclusions was more significant.

(3) Similar to the BS, the grains in the adjacent BSs formed the MBS and transformed into the martensite phase during the cooling process, instead of retaining their ferrite phase. This is because the concentration of the segregated elements (Cr) in the MBS was not sufficient to stabilize the microstructure.

(4) The MnS inclusions played the role of pinning and refining the grains and showed four types of distribution, namely between two grain boundaries, between polycrystalline boundaries, within the grains, and throughout the grains.

References

1. Wu X, Wu L, Xie J, Shen P, Fu J (2020) Metall Res Technol, 117(107) pp (1–8)
2. Domizzi G, Anteri G, Ovejero-Garcia J (2001) Corros Sci 43:325–339
3. You D, Michelic SK, Bernhard C, Loder D, Wieser G (2016) ISIJ Int 56:1770–1778
4. Miettinen J (2000) Metall Mater Trans B 31B:365–379
5. Matsunaga T, Hongo H, Tabuchi M, Sahara R (2016) Mater. Sci. Eng. A-Struct. 655:168–174
6. Chi HX, MA DS, Xu HX, Zhu WL, Jiang JQ (2016) J Iron Steel Res. Int, 23, pp 484–88
7. Wang K, Yu T, Song Y, Li H, Liu M, Luo R, Zhang J, Fang F, Lin X (2019) Metall Mater Trans B 50B:1213–1224